

A Coupled Model for Three-Phase Capillary Pressure and Relative Permeability

Odd Steve Hustad,* SPE, SINTEF Petroleum Research

Summary

A fully coupled formulation for three-phase capillary pressure and relative permeability is presented. The formulation incorporates hysteresis and miscibility on both capillary pressure and relative permeability, simultaneously. Consistency is ensured for all three two-phase boundary conditions through the use of two-phase data and the application of normalized saturations.

Simulation examples of water-alternating-gas (WAG) injection are demonstrated using water-, mixed-, and oil-wet capillary pressure and relative permeability curves, both exhibiting hysteresis. The examples represent typical core-flooding scales in the centimeter to meter range. Discussions and illustrations are given demonstrating the importance of the functional dependency and the extrapolation of two-phase capillary pressure values to three-phase flow properties.

Introduction

Many papers have been written addressing the problem of three-phase relative permeability and capillary pressure. Literature review of various models is well documented elsewhere. See Refs. 1 through 8, along with their references. Likewise, for documentation of experimental observations, see Refs. 9 through 17.

One three-phase formulation that has been suggested is such that each phase's property is dependent on all three saturations.¹⁸ This formulation is extended here to include hysteresis and miscibility, where hysteresis may be applied to any of the two-phase properties.

Models are usually developed to address specific reservoir needs for the modeling of recovery processes, such as gas injection after waterflooding, WAG injection, or pressure blowdown after waterflooding. These models may be generalized to be applicable for other processes and reservoirs. When considering three-phase flow, models usually have been developed for relative permeability to oil, often assumed to be the intermediate wetting phase. These models combine two-phase data in various forms, making them dependent on two saturations, gas and water. Relative permeabilities to gas and water are usually made dependent on each phase's saturation, because they are often considered as the nonwetting and wetting phases, respectively. Gas-oil and oil-water capillary pressures are dependent on gas and water saturations, respectively. It is usually assumed that gas-water capillary pressure is the sum of the other two capillary pressures.¹⁹ Hysteresis has also been suggested for both relative permeability and capillary pressure.^{4,7,8,14,20}

Motivation. The motivation for developing an alternative three-phase formulation for reservoir simulation lies first of all in the difficulty of reproducing coreflooding results with reservoir simulators. Commonly used formulations like those of Stone²¹ have been successfully applied, although some questions may be raised when applying the same formulation to more than one process having convective flow with and without vaporization.²² Ref. 22 presents two gas displacement experiments in vertical cores after

waterflooding and their associated numerical modeling. The modeling of the first experiment, in which equilibrium gas to oil is injected, achieved an acceptable match of the recoveries with minor adjustments to Stone's first model. However, applying the capillary pressure and relative permeability model and data to model the similar second experiment, dry gas injection, did not result in satisfactory recoveries. In fact, the water recovery (wetting phase) was the one most in error.

Simulations of coreflooding experiments have demonstrated that the saturation profiles are strongly dependent on the capillary forces and on the boundary conditions at the inlet and outlet of the core.^{18,22}

Oak *et al.*¹⁷ concluded that relative permeability depends on fluid saturation and on the saturation history. The proposed model should therefore have capillary pressure and relative permeability values that are saturation history-dependent. That is, the properties assigned to the capillary pressure and relative permeability for a particular set of three-phase saturations should not be unique, but dependent on the saturation history leading up to the three-phase saturation condition.

An example in which modeling problems may arise for the state-of-the-art modeling of three phases is when a first-contact miscible injection process causes an oil-water system to become a gas-water system. The problem relates to the labeling of the hydrocarbon phase. Discontinuous relative permeability to hydrocarbon phase may occur when the phase label changes. Consistency may also be violated if incorrect gas-water capillary pressure and endpoint saturation values are applied.

The use of normalized saturation to model scanning two-phase capillary pressure curves have been successfully applied by Kleppe *et al.*¹⁴ Their model is based on the fact that the scanning capillary pressure curves lie between two limiting scanning curves and converge at the same endpoint saturation.¹⁶

The proposed model should ensure that capillary pressure and relative permeability are consistent and continuous for flow processes that go from any two-phase state to another two-phase state by way of the three-phase state.

Another motivation for this model is that the user should apply the "true" two-phase data, while the three-phase formulation should incorporate these data in a manner that most correctly estimates the three-phase properties.

It has been observed from centrifuge measurements that different fluid pairs will result in different endpoint saturations.²² A distinction should therefore be made between the terms "residual" and "endpoint" saturations. The endpoint saturation is defined here as the smallest obtainable saturation where the phase is still continuous. The endpoint saturation also represents the saturation where the relative permeability becomes zero. For saturation values at and below the endpoint saturation, the phase is discontinuous.

Residual saturation, on the other hand, represents the saturation where a phase becomes immobile. This condition may arise for different capillary pressure values, depending on the phase's pressure gradient or how high (or low) capillary pressure is achieved by the flow conditions. The relative permeability need not be zero at this condition, but for no flow to occur the phase pressure gradients (phase potentials) must be zero. By these definitions, the residual saturation is therefore greater than or equal to the endpoint saturation.

Endpoint and residual-saturation terms should also incorporate information about processes that have been subjected to upscaling. Here, the endpoint saturation may be related to the upscaled pro-

* Now with Statoil.

Copyright © 2002 Society of Petroleum Engineers

This paper (SPE 74705) was revised for publication from paper SPE 63150, first presented at the 2000 SPE Annual Technical Conference and Exhibition, Dallas, 1–4 October. Original manuscript received for review 27 October 2000. Revised manuscript received 10 May 2001. Manuscript peer approved 18 May 2001.

cess for a gridblock. In such cases, process-dependent endpoint saturations may include sweep efficiency of the volume represented by the gridblock, and one can apply a formulation as suggested by Land.²³ This requires a separate handling of these terms for the gridblock and the rock-type dependent input values. The Land formulation may be applied to the gridblock values, while the rock-type dependent input values may be applicable to many gridblocks with varying absolute permeabilities.

Presented below is the proposed two-phase model, how the two-phase data are related between input and gridblock values, the hysteresis formulation on capillary pressure and relative permeability, and the miscibility formulation. The proposed three-phase model is then presented, demonstrating how representative two-phase properties are extrapolated to three-phase properties. WAG injection simulation examples are demonstrated for various wetting conditions using typical capillary pressure and relative permeability curves, both exhibiting hystereses. Finally, examples are given for first-contact miscible WAG injection with the three data sets representing the different wetting conditions.

Two-Phase Formulation

The formulation is constructed such that it permits one to operate with various forms of normalized saturations. Normalization is applied to saturation values from input and gridblock, as well as process-dependent hysteresis saturations.

Two-phase data are entered on input. The saturations are functions of capillary pressure. The two-phase relative permeabilities are functions of saturation. The two-phase properties are also made dependent on their interfacial tension (IFT), relating the entered values to a reference interfacial tension.

The hysteresis formulation is based on two limiting scanning curves for increasing and decreasing saturations. The capillary pressure is made continuous for processes having a change in saturation direction through a rescaling of the saturation range. For the saturation direction change of a particular process, the saturations are renormalized based on the process-dependent endpoint saturation and turning-point saturation. The relative permeabilities are also made continuous by applying the same normalized saturations as for the capillary pressure.

Input. On input, oil-water and gas-oil two-phase data are entered into the simulator where the functional dependency is as follows:

$$\check{S}_w = \check{S}_w(\check{P}_{cow}), \quad (1)$$

$$\check{S}_g = \check{S}_g(\check{P}_{cgo}), \quad (2)$$

and

$$\check{k}_{rwo} = \check{k}_{rwo}(\check{S}_w); \quad \check{k}_{row} = \check{k}_{row}(\check{S}_w) \quad (3)$$

$$\check{k}_{rgo} = \check{k}_{rgo}(\check{S}_g); \quad \check{k}_{rog} = \check{k}_{rog}(\check{S}_g). \quad (4)$$

The input saturations are normalized with respect to their endpoint saturations by

$$\check{S}_i = \frac{\check{S}_i - \check{S}_{iro}}{1 - \check{S}_{ori} - \check{S}_{iro}}, \quad i = g, w. \quad (5)$$

A ternary illustration of the saturation space with the two-phase relative permeability and endpoint saturations is shown in **Fig. 1**. Included in the figure are the gas-water system's relative permeabilities and endpoint saturations, which are not required on input.

Gridblock. There may be several sets of input data representing different rock types, and each simulation gridblock must be assigned one such data set. Each gridblock must also be assigned six reference endpoint saturations, denoted by

$$\bar{S}_{gro}^r, \bar{S}_{grw}^r, \bar{S}_{org}^r, \bar{S}_{orw}^r, \bar{S}_{wrg}^r \text{ and } \bar{S}_{wro}^r. \quad (6)$$

For processes exhibiting two-phase flow, the simulation gridblock saturations may be normalized using Eq. 5, where the endpoint saturations and saturations are those pertaining to the gridblock.

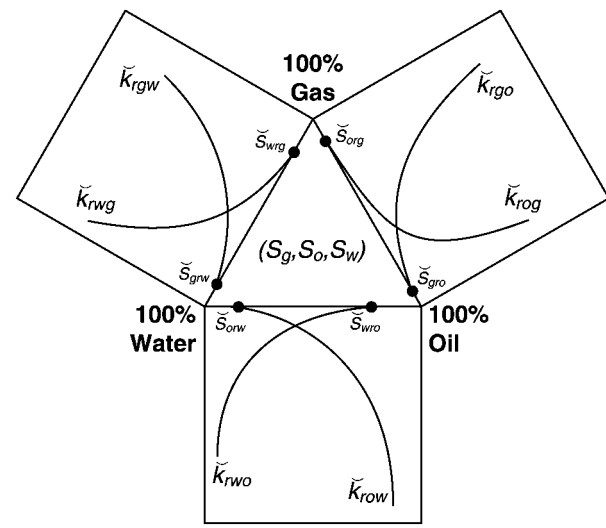


Fig. 1—Ternary representation of saturation space with two-phase relative permeability.

The oil-water data is used to represent the gas-water system. This representation ensures consistency when miscibility and hydrocarbon phase labeling changes occur. This is discussed further under miscibility. For the gas-water system, Eq. 5 must be replaced by

$$S_w = \frac{\bar{S}_w - \bar{S}_{wrg}}{1 - \bar{S}_{grw} - \bar{S}_{wrg}}. \quad (7)$$

The gridblock endpoint saturation, \bar{S}_{ijr} , may also be made dependent on interfacial tension (miscible processes) where

$$\bar{S}_{ijr}^m = \bar{S}_{irg}^r \cdot f_{ij} \quad (8)$$

and

$$f_{ij} = \left(\frac{\sigma_{ij}}{\sigma_{ij}^r} \right)^{n_{ij}}. \quad (9)$$

σ_{ij} represents the interfacial tension between the phases i and j , superscript r refers to a reference state, and n_{ij} =a user-specified constant. Depending on the displacement process, Eq. 9 may be different for different intervals of interfacial tension, and a different formulation may be more appropriate.^{3,5} Note also that there are two reference states, that of the input data and that of the gridblock. These are assumed to be equal hereinafter.

The gridblock endpoint saturations may also be process-dependent.^{5,23} This is most relevant for the gas phase. It may be sufficient to apply a Land-type relation such as

$$\bar{S}_{ijr} = \frac{\bar{S}_i^{\max}}{1 + \frac{\bar{S}_i^{\max}}{\bar{S}_{ijr}^m} - \frac{\bar{S}_i^{\max}}{1 - \bar{S}_{jri}^m}} \quad (10)$$

where $i \neq j$, \bar{S}_i^{\max} = the maximum i -phase saturation experienced by the gridblock, and \bar{S}_{ijr}^m and \bar{S}_{jri}^m = the gridblock endpoint saturations, defined by Eq. 8. Note, the following condition must be fulfilled for Eq. 10,

$$\bar{S}_i^{\max} \leq 1 - \bar{S}_{jri}^m. \quad (11)$$

Because both the input and gridblock saturations are normalized to values between zero and one, they may be applied on a one-to-one basis to allocate gridblock capillary pressure and relative permeability values from input values.

Hysteresis. The hysteresis formulation requires two sets of saturation functions of Eqs. 1 and 2, one for increasing and another for decreasing saturations. The increasing and decreasing saturations represent the process direction due to flow. To illustrate the principles behind the formulation, **Fig. 2** shows a process that goes

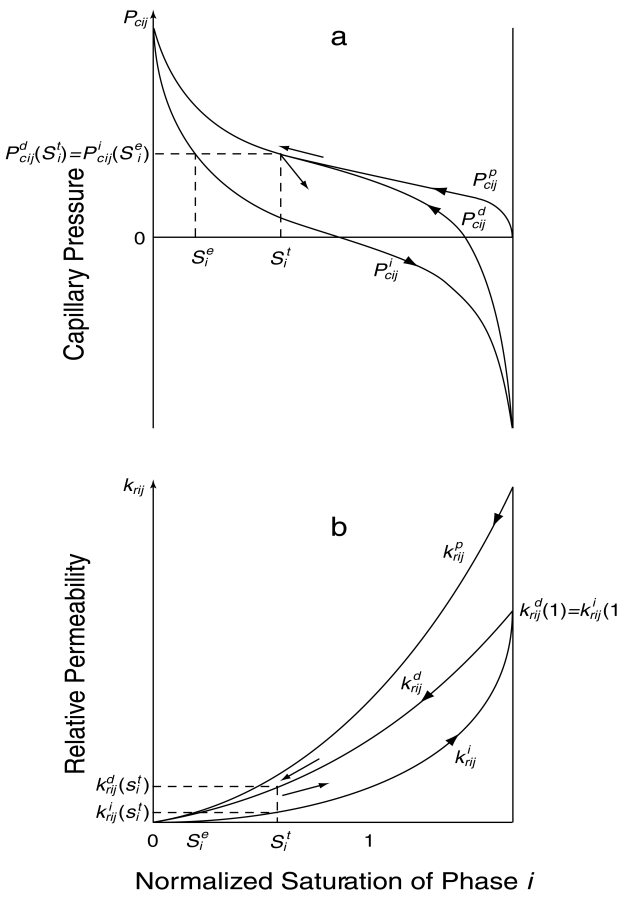


Fig. 2—Hysteresis capillary pressure and relative permeability for process switching from decreasing to increasing saturations.

from decreasing to increasing saturation. At the turning-point saturation, \bar{S}_i^t , the formulation ensures that the capillary pressure is continuous. This is achieved by rescaling the increasing saturation range. At the turning-point saturation, \bar{S}_i^t , an equivalent saturation value, S_i^e , is found for the increasing saturation function where its capillary pressure has the same value as for the decreasing saturation function. Thereafter, the normalized hysteresis saturation is determined for the continued process with increasing saturations, where the turning-point and equivalent saturations are applied as constants:

$$S_i^h = S_i^e + (S_i - S_i^t) \left(\frac{1 - S_i^e}{1 - S_i^t} \right), \quad S_i \geq S_i^t \quad \dots \quad (12)$$

where $i=g,o,w$.

This normalized hysteresis saturation scaling has the effect of compressing the saturation range for the capillary pressure curve (increasing saturation, from equivalent saturation to one) into the saturation range from the turning-point saturation to its maximum value of one. Note that both the turning point and equivalent saturations are normalized values and that they are kept fixed as long as the process direction continues (increasing saturation).

The turning point and equivalent saturations are recalculated when the process direction changes to decreasing saturations. For decreasing saturations, the normalized hysteresis saturation takes the form

$$S_i^h = S_i \left(\frac{S_i^e}{S_i^t} \right), \quad S_i \leq S_i^t, \quad i = g,o,w. \quad \dots \quad (13)$$

The equivalent saturation, S_i^e , represents a saturation value for the decreasing saturation function, in which the capillary pressure is equal to the value at the turning-point saturation.

From the normalized hysteresis saturation, S_i^h , the two-phase capillary pressure can be determined by equating the normalized hysteresis saturation to the normalized input saturation and allo-

cating the capillary pressure value to the gridblock. This procedure ensures continuity for the capillary pressure. Note that the capillary pressure derivative with respect to saturation will have a discontinuity at the turning-point saturation.

The relative permeability to phases i and j for a process with increasing saturation is determined by

$$\tilde{k}_{rji}(S_i) = k_{rji}^d(S_i^t) + [k_{rji}^i(S_i^h) - k_{rji}^i(S_i^e)] \left[\frac{k_{rji}^i(1) - k_{rji}^i(S_i^t)}{k_{rji}^i(1) - k_{rji}^i(S_i^e)} \right] \quad \dots \quad (14)$$

and

$$\tilde{k}_{rji}(S_i) = k_{rji}^i(S_i^h) \left[\frac{k_{rji}^d(S_i^t)}{k_{rji}^i(S_i^e)} \right]. \quad \dots \quad (15)$$

k_{rji}^d and k_{rji}^i represent the input relative permeability for decreasing and increasing saturations, respectively, where the saturation scale has been normalized.

For a process with decreasing saturation, the relative permeabilities are

$$\tilde{k}_{rji}(S_i) = k_{rji}^d(S_i^h) \left[\frac{k_{rji}^i(S_i^t)}{k_{rji}^d(S_i^e)} \right] \quad \dots \quad (16)$$

and

$$\tilde{k}_{rji}(S_i) = k_{rji}^i(S_i^h) + [k_{rji}^d(S_i^h) - k_{rji}^d(S_i^e)] \left[\frac{k_{rji}^d(0) - k_{rji}^d(S_i^t)}{k_{rji}^d(0) - k_{rji}^d(S_i^e)} \right]. \quad \dots \quad (17)$$

Eqs. 14 and 17 will result in relative permeability curves that run parallel with the limiting (input) scanning relative permeability curve. Eqs. 15 and 16 ensure that the relative permeability becomes zero at normalized saturation equal to zero.

Notice that the phase properties are dependent on the phase's own normalized saturation. Earlier attempts to code this proposed model have demonstrated that if consistency is to be ensured for three-phase conditions, each phase's relative permeability must be made dependent on the phase's normalized saturation.²⁴

Miscibility. To ensure consistency at miscible conditions, the capillary pressure is scaled by the interfacial tensions using Eq. 9,

$$\hat{P}_{cij} = f_{ij} \cdot \tilde{P}_{cij}. \quad \dots \quad (18)$$

Likewise, the relative permeability is scaled by

$$\hat{k}_{rji} = f_{ij} \cdot \tilde{k}_{rji} + (1 - f_{ij}) \cdot S_i, \quad f_{ij} \leq 1$$

$$\hat{k}_{rji} = \tilde{k}_{rji}, \quad f_{ij} > 1, \quad \dots \quad (19)$$

where S_i = the normalized gridblock saturation.

The two hydrocarbon and the two water endpoint saturations for the two hydrocarbon-water systems must also be equal at equal interfacial tensions. The following equations have been applied to the examples below:

$$\bar{S}_{irw} = \bar{S}_{irw}^m \pm \frac{h}{2} |S_{grw} - S_{orw}|, \quad i = g,o, \quad \dots \quad (20)$$

and

$$\bar{S}_{wri} = \bar{S}_{wri}^m \pm \frac{h}{2} |S_{wrg} - S_{wrd}|, \quad i = g,o, \quad \dots \quad (21)$$

where

$$h = 0, \quad |\sigma_{gw} - \sigma_{ow}| \geq \Delta\sigma^{\max} \text{ and}$$

$$h = \Delta\sigma^{\max} + |\sigma_{gw} - \sigma_{ow}|, \quad |\sigma_{gw} - \sigma_{ow}| < \Delta\sigma^{\max}. \quad \dots \quad (22)$$

Three-Phase Formulation

The three-phase properties are based on representative two-phase properties, which are combined through a weighing scheme of the saturations to obtain the three-phase properties.¹⁸ Each phase property is made dependent on its own normalized saturation to ensure consistency. That is, zero relative permeability is ensured at and below the endpoint saturation.^{24,25} Three sets of two-phase values

are applied, allowing variable endpoint saturations within the three-phase space.

Based on the three gridblock saturations and the six gridblocks' endpoint saturations, minimum and maximum saturations are determined for each phase. The minimum and maximum saturations for phase i can be obtained as follows.

Let the saturations of phases j and k represent the coordinates in a rectangular coordinate system. The axes represent the boundary between the two-phase and three-phase states. The four endpoint saturations, S_{irj} , S_{irk} , S_{jri} , and S_{kri} are placed on their respective axis locations, namely $(S_{jri}, 0)$ and $(1-S_{irj}, 0)$ on the x -axis, and $(0, S_{kri})$ and $(0, 1-S_{irk})$ on the y -axis. Join the endpoint saturations S_{irj} and S_{irk} with a straight line. Likewise, join S_{jri} and S_{kri} . These lines represent the minimum and maximum saturation boundaries in which phase i is mobile. Given the gridblock saturations represented by the point (S_j, S_k) , draw a straight line through this point and the apex of phase i , point $(0,0)$. This last line will intersect the first two lines at values given by Eqs. 23 and 24 respectively. Because there is symmetry in the formulation, the minimum and maximum saturations of phase i are then given by¹⁸

$$\bar{S}_{imn} = \frac{\bar{S}_j \bar{S}_{irj} + \bar{S}_k \bar{S}_{irk} + \bar{S}_{irj} \bar{S}_{irk} (\bar{S}_i - 1)}{\bar{S}_j (1 - \bar{S}_{irk}) + \bar{S}_k (1 - \bar{S}_{irj})} \quad \dots \dots \dots \quad (23)$$

and

$$\bar{S}_{imx} = \frac{\bar{S}_j \bar{S}_{kri} + \bar{S}_k \bar{S}_{jri} + \bar{S}_{jri} \bar{S}_{kri} (\bar{S}_i - 1)}{\bar{S}_j \bar{S}_{kri} + \bar{S}_k \bar{S}_{jri}}, \quad \dots \dots \dots \quad (24)$$

where subscripts i , j , and k represent either the gas, oil, or water phase, and $i \neq j \neq k$. It may be emphasized that the first two lines need not necessarily be straight lines. They may have a concave or convex shape, but they must result in unique intersection points with the straight line going through the saturation point and the i -phase apex.

The gridblock saturations are then normalized by

$$S_i = \frac{\bar{S}_i - \bar{S}_{imn}}{\bar{S}_{imx} - \bar{S}_{imn}}, \quad i = g, o, w. \quad \dots \dots \dots \quad (25)$$

Note that for a three-phase condition, the normalized saturations from Eq. 25 do not sum to unity, as they do for two-phase conditions.

Based on the normalized saturations from Eq. 25, six hysteresis-normalized saturations are determined from either Eq. 12 or 13, depending on the process saturation direction, two for each phase, relating to the three two-phase pairs. Representative two-phase values, from input values, are then selected based on these normalized hysteresis saturations.

The gas phase's representative two-phase value, for the gas-oil system, is determined in a straightforward manner. However, to obtain the gas phase's representative value from the gas-water system, the normalized hysteresis gas saturation has to be changed to hysteresis water saturation by

$$\hat{S}_w^h = 1 - S_g^h. \quad \dots \dots \dots \quad (26)$$

This is to ensure the same phase labeling between the input data and the gridblock-normalized hysteresis saturation.

For the oil phase, the normalized hysteresis oil saturation must be made compatible with the input normalized saturations by setting

$$\hat{S}_w^h = 1 - S_o^h \quad \dots \dots \dots \quad (27)$$

for the oil-water system, and

$$\hat{S}_g^h = 1 - S_w^h \quad \dots \dots \dots \quad (28)$$

for the gas-oil system before obtaining the representative two-phase oil phase values. For the water-phase representative value, the procedure is straightforward for both oil-water and gas-water systems, in which the normalized hysteresis water saturation is used directly.

The above procedure leads to the following representative two-phase capillary pressure values,

$$\tilde{P}_{cgo}(S_g^h), \tilde{P}_{cgo}(\hat{S}_g^h), \tilde{P}_{cgw}(\hat{S}_w^h), \tilde{P}_{cgw}(S_w^h), \tilde{P}_{cow}(\hat{S}_w^h), \tilde{P}_{cow}(S_w^h), \dots \quad (29)$$

and the representative two-phase relative-permeability values are

$$\tilde{k}_{rgo}(S_g^h), \tilde{k}_{rgo}(\hat{S}_w^h), \tilde{k}_{rog}(\hat{S}_g^h), \tilde{k}_{row}(\hat{S}_w^h), \tilde{k}_{rwg}(S_w^h), \tilde{k}_{rwo}(S_w^h). \quad \dots \dots \dots \quad (30)$$

Notice that this procedure generates two representative capillary pressure values for each set of phase pairs. The two representative capillary pressures are dependent on one of the two normalized saturations. The choice of representative capillary pressure from Eq. 29 is still a subject for further research and is revisited in the examples below.

The representative capillary pressure from Eq. 29 may be made dependent on interfacial tension through the use of Eq. 18. Likewise, the representative relative permeability may be made interfacial tension-dependent through the use of Eq. 19.

To ensure consistency in capillary pressure, Hustad and Hansen¹⁸ suggested a saturation dependency among three two-phase capillary pressures. This criterion can be generalized further as follows.

For three-phase conditions, the capillary pressures must satisfy the following equation,

$$P_{cgw} - P_{cgo} - P_{cow} = 0. \quad \dots \dots \dots \quad (31)$$

When representative values of the capillary pressures are determined, Eq. 31 is not necessarily fulfilled and a residual R is obtained, hence

$$\hat{P}_{cgw} - \hat{P}_{cgo} - \hat{P}_{cow} = R. \quad \dots \dots \dots \quad (32)$$

To satisfy Eq. 31, the functions F , G , and H are introduced, having the property

$$F + G + H = 1. \quad \dots \dots \dots \quad (33)$$

The representative capillary pressures may be modified by

$$P_{cgo} = \hat{P}_{cgo} + F \cdot R, \quad \dots \dots \dots \quad (34)$$

$$P_{cgw} = \hat{P}_{cgw} - G \cdot R, \quad \dots \dots \dots \quad (35)$$

and

$$P_{cow} = \hat{P}_{cow} + H \cdot R, \quad \dots \dots \dots \quad (36)$$

fulfilling Eq. 31.

The functions in Eq. 33 are dependent on saturation. In addition, Eq. 33 may also be dependent on interfacial tension, wettability, and possibly other factors. This may be most important at low saturations. For example, when the intermediate phase saturation becomes extremely low, the curvature of the two two-phase interfaces may have an influence on one another. Another possibility is that the intermediate phase may rupture, causing the wetting and nonwetting phases to be in direct contact.

For demonstration purposes, the following functional relationship has been selected,

$$F = \frac{\delta_w \bar{S}_w^{\alpha_w}}{\bar{S}_w^{\alpha_w} + (1 - \bar{S}_w)^{\beta_w}}, \quad \dots \dots \dots \quad (37)$$

$$H = \frac{\delta_g \bar{S}_g^{\alpha_g}}{\bar{S}_g^{\alpha_g} + (1 - \bar{S}_g)^{\beta_g}}, \quad \dots \dots \dots \quad (38)$$

and

$$G = 1 - F - H. \quad \dots \dots \dots \quad (39)$$

The phase pressures are related by

$$P_o = p$$

$$P_g = p + P_{cgo}$$

$$P_w = p - P_{cow}. \quad \dots \dots \dots \quad (40)$$

The three-phase relative permeabilities are determined by weighing the representative values by the gridblock saturations,

$$k_{ri} = \frac{\bar{S}_j}{\bar{S}_j + \bar{S}_k} \hat{k}_{rij} + \frac{\bar{S}_k}{\bar{S}_j + \bar{S}_k} \hat{k}_{rik}, \quad \dots \dots \dots \quad (41)$$

where $i = g, o, w$ and $i \neq j \neq k$.

This formulation permits proper modeling of the two-phase mirror image of the three-phase process. Continuity is also ensured for processes going from a three-phase state to any two-phase state. In addition, for a particular three-phase saturation direction, the two-phase mirror image (say, for the oil phase) may be an increasing oil saturation process for the representative two-phase gas-oil system and a decreasing oil saturation process for the other representative two-phase oil-water system.⁸

Calculation Procedure

A calculation procedure is summarized for a typical three-phase condition. An IMPES-type simulator formulation is assumed, in which the properties are kept constant over a timestep. At the end of a timestep, six saturation direction pointers are set. If a saturation direction has changed, new equivalent saturation and turning-point saturation are determined. The current relative permeabilities (not scaled by IFT) are also stored, in case the saturation direction should change. If the saturation direction changes over the timestep, the stored relative permeabilities will be the turning-point relative permeability at the turning-point saturation for the continued process.

Given the gridblock's three saturation values and three interfacial tension values at the start of a timestep, the phase's capillary pressure and relative permeability are determined as follows:

1. Set the IFT scaling factor, Eq. 9.
2. Set the six gridblock endpoint saturations, Eq. 10, and multiply by IFT scaling factor, Eq. 8.
3. Calculate the normalized saturations, Eqs. 23 through 25.
4. Determine the normalized hysteresis saturation, Eq. 12 or Eq. 13.
5. Set the appropriate normalized saturation, Eqs. 26 through 28, and look up representative capillary pressure and relative permeability values, Eq. 29 and Eq. 30, respectively.
6. Scale capillary pressure and relative permeability values with IFT scaling factor, Eq. 18 and Eq. 19.
7. Set gridblock phase relative permeability values, Eq. 41.
8. Correct capillary pressures, Eqs. 34 and 36, to ensure Eq. 31, and allocate values to the gridblock.

Examples and Discussions

A reservoir trap is, historically, initially 100% water saturated prior to hydrocarbon migration into the trap. The hydrocarbons migrating into the trap displace the water (primary drainage or first decreasing water saturation cycle) to residual water saturation. Furthermore, as time progresses, the reservoir matures and may change its wettability and saturation distribution. After discovery, various processes may be applied to deplete the hydrocarbons from the reservoir.

A homogeneous, 1D horizontal segment of a fictitious oil column is chosen to demonstrate the above formulation. The assumption is made that the flooding process occurs horizontally along the 1D segment. Model parameters for the immiscible simulations are listed in **Table 1**.

The producing well is located in the last gridblock (100), the water injector in the second gridblock, and the gas injector in the first gridblock. The production well is kept at a constant bottom-hole pressure of 344 bar, and the injection wells are kept at constant reservoir injection rates.

The reservoir oil (and gas) is modeled by the Soave-Redlich-Kwong equation of state, and the model parameters are those from Table 2 of Ref. 26. The injection gas composition, for the immiscible processes, is the equilibrium gas to the oil at the bubblepoint

TABLE 1—DATA USED IN IMMISCIBLE EXAMPLES

| Parameter | Value |
|--|-------------------|
| Permeability (md) | 500 |
| Porosity (%) | 25 |
| Length (cm) | 342 |
| Pore volume (cm ³) | 1000 |
| Initial water volume (cm ³) | 150 |
| Initial fluid densities $g-o-w$ (g/cm ³) at 345 bar | 0.287–0.519–0.994 |
| Initial fluid viscosities $g-o-w$ (cp) at 345 bar | 0.037–0.146–0.305 |
| Initial and reference IFT's $g_o-g_w-g_w$ (mN/m) | 0.0648–32.9–26.1 |
| All IFT exponent terms n_{ij} in Eq. 9 | 1 |
| Rock compressibility (bar ⁻¹) | 0.00007 |
| Average water compressibility (bar ⁻¹) | 0.0005 |
| Reservoir temperature (°C) | 140 |

pressure. The gas-oil interfacial tension is modeled according to Ref. 27. The hydrocarbon-water interfacial tensions are modeled by

$$\sigma_{hw} = A(\Delta\rho)^2 + B\Delta\rho + C, \quad i = g, o \quad \dots \dots \dots \quad (42)$$

where A , B , and C are constants and

$$\Delta\rho = \rho_w - \rho_i, \quad i = g, o \quad \dots \dots \dots \quad (43)$$

Caution should be exercised when applying Eq. 42 to other fluid systems. For the examples below, values of 20, 1, and 15 are given to the constants A , B , and C respectively. The spreading coefficients for the examples below are positive, representing a spreading system. $\Delta\sigma^{\max}$ is set to unity in Eq. 22.

Alternating equal reservoir volumes of water and gas in cycles of 15 hours each floods the 1D segment. The rates are 10 cm³/h. Therefore, 15% of the segment's total pore volume is flooded by each injection cycle. The segment is first flooded by water, followed by gas, then water, and so on.

The capillary pressure and relative permeability curves are shown in **Figs. 3 through 5** for water-, mixed-, and oil-wet systems respectively. No significance should be given to these curves other than that they have representative features typical for the wetting conditions. Hysteresis has been assigned to all curves for illustration purposes. A feature to be aware of is that the relative permeability value for increasing water saturation lies below those for decreasing saturation. This is contrary to some other findings.^{12,13}

The first flooding cycle is a two-phase waterflood. The increasing water saturation's capillary pressure and relative permeability values (oil-water system) relating to the hysteresis loop are therefore applied for the water- and mixed-wet systems. Primary increasing water saturation data is used for the oil-wet system before switching to data representing the hysteresis loop. This is done to ensure consistency with the chosen endpoint saturations (**Table 2**). Endpoint saturations in Table 2 are also used as the reference gridblock endpoint saturations (Eq. 6).

The first gas-injection cycle will apply a primary gas-oil data set, labeled S_g^P (**Figs. 3 through 5**), before switching to the hysteresis loop, labeled S_g^d and S_g^i for decreasing and increasing gas saturations, respectively. The criteria for switching from the primary relative permeability curve to the hysteresis loop are that the primary value must be lower than the maximum hysteresis value, and that the process saturation direction must have changed.

Figs. 6 through 8 illustrate saturation vs. normalized length at the end of each injection cycle for the water-, mixed- and oil-wet examples respectively. As may be expected, the three examples vary in their saturation profiles.

These examples show that the gas front advances faster for the water-wet example compared to the mixed- and oil-wet examples,

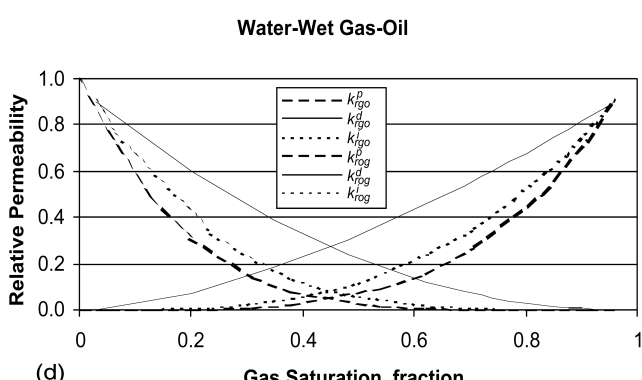
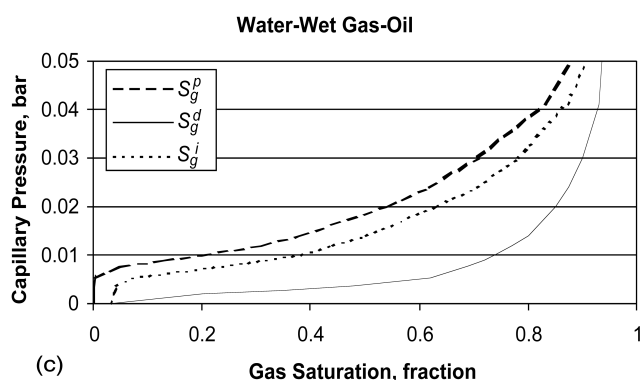
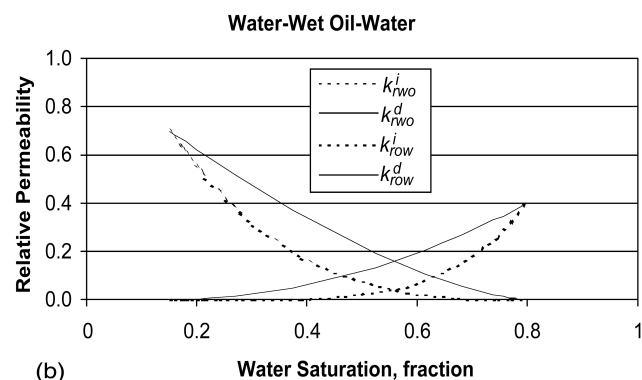
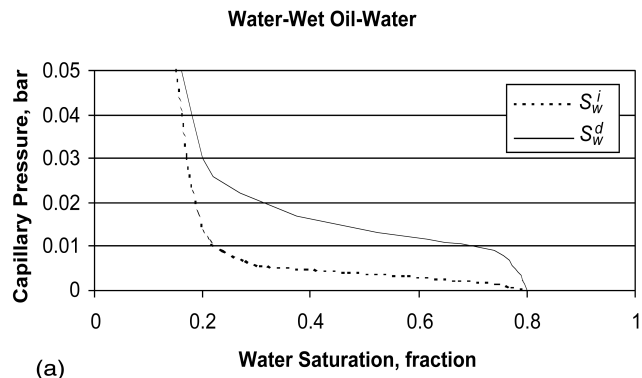


Fig. 3—Capillary pressure and relative permeability data for water-wet system.

and that the water front advances slower for the water-wet compared to the mixed- and oil-wet examples.

In the above three examples, the capillary pressure (Eq. 29) was modeled by

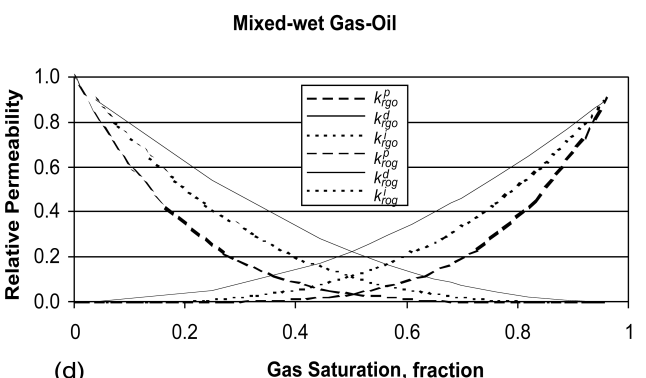
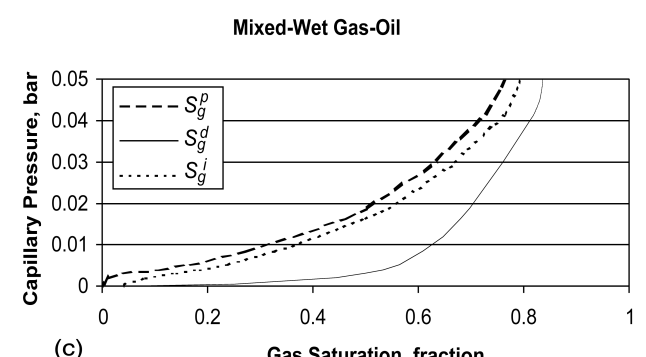
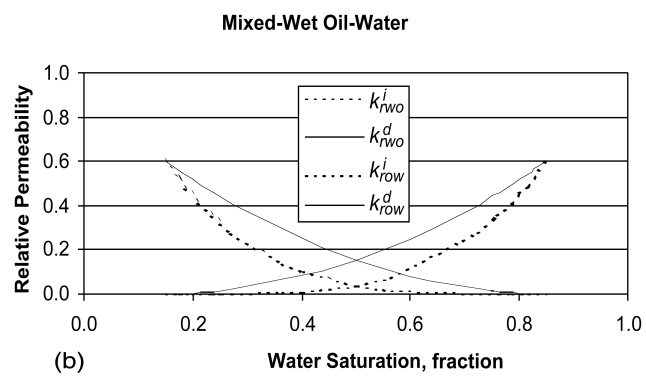
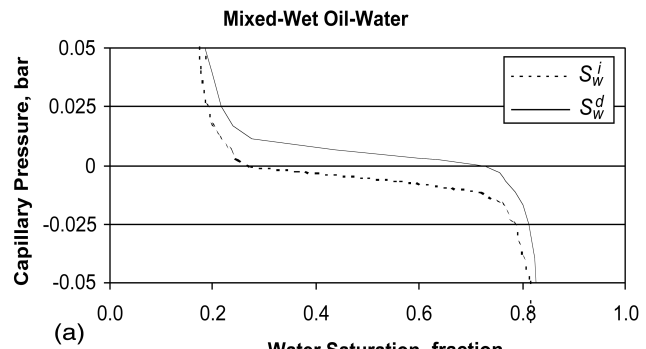


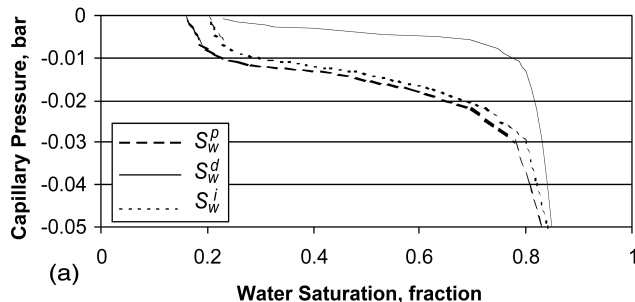
Fig. 4—Capillary pressure and relative permeability data for mixed-wet system.

and

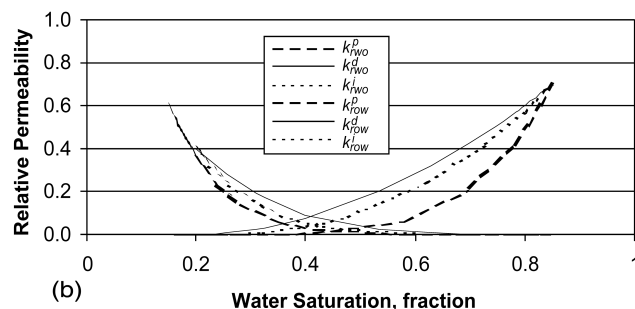
δ_g and δ_w were set to zero in Eqs. 38 and 37.

To demonstrate the importance of the functional relationship of capillary pressure on saturation, and its impact on saturation pro-

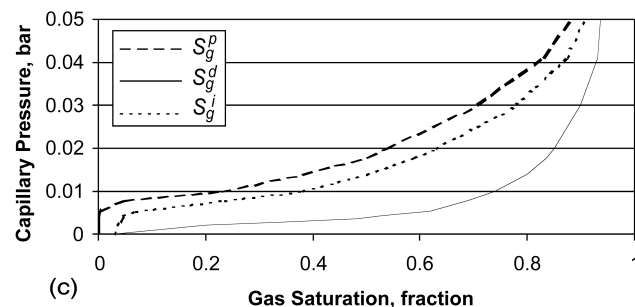
Oil-Wet Oil-Water



Oil-Wet Oil-Water



Oil-Wet Gas-Oil



Oil-Wet Gas-Oil

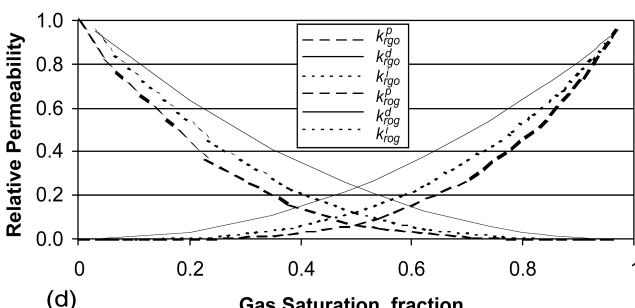


Fig. 5—Capillary pressure and relative permeability data for oil-wet system.

files, Eqs. 37 and 38 have been applied together with the water-wet data (Fig. 3). Two parameter sets of functions F and H are listed in Table 3.

Fig. 9 shows the saturation profiles obtained at the end of the first gas-injection cycle. Comparing these profiles with Fig. 6b, one will notice that the gas-front saturation has a higher value. The choice of parameters in the functions F and H also results in different saturation profiles.

TABLE 2—ENDPOINT SATURATIONS FOR EXAMPLES

| Endpoint Saturation | Water-wet | Mixed-wet | Oil-wet |
|---------------------|-----------|-----------|---------|
| S_{ow} | 0.20 | 0.15 | 0.15 |
| S_{wro} | 0.15 | 0.15 | 0.20 |
| S_{gro} | 0.03 | 0.04 | 0.03 |
| S_{org} | 0.04 | 0.04 | 0.03 |
| S_{grw} | 0.06 | 0.04 | 0.03 |
| S_{wrg} | 0.05 | 0.045 | 0.04 |

In Fig. 9b, the gas-front saturation profile has an erratic profile, whereas the profile in Fig. 9a is smooth. In the few examples that have been tested so far, erratic saturation profiles do occur for certain combinations of capillary pressures. The capillary pressure scaling with interfacial tension can also lead to smoother or more erratic saturation profiles. However, these erratic saturation profiles do not necessarily create any numerical difficulties for the simulations, but may influence the timestepping procedure.

The erratic saturation profiles are the result of the solution of the pressure equation. If the converged solution for the gridblock pressure, p , oscillates from gridblock to gridblock, so will the saturations. Either decreasing the tolerance for the convergence criteria of the pressure equation or reducing the timestep size may resolve this problem.

Fig. 10 shows two resulting saturation profiles for the mixed- and oil-wet rock curves. In these runs, the capillary pressures were modeled by

$$\tilde{P}_{cgw} = \tilde{P}_{cgw}(S_w^h) - \tilde{P}_{cow}(\hat{S}_w^h) \quad (46)$$

and

$$\tilde{P}_{cow} = \tilde{P}_{cow}(\hat{S}_w^h). \quad (47)$$

The functions F and H (Eqs. 37 and 38) were zero.

Comparing Fig. 10a with Fig. 7c, one can observe in Fig. 10a that the water-front is slightly more advanced, the gas saturation front is not as far advanced, and that the gas has a much larger front saturation.

Comparing Fig. 10b with Fig. 8c, the difference is not that significant, even though the water saturation profiles are slightly different. The profiles in Fig. 10b are not as smooth. These irregularities can partly be caused by linear interpolation of table lookup values.

The functional relationship of two-phase data to three-phase data is still a subject for further research, and this model should only be interpreted as a simple interpolation scheme of two-phase data to three-phase conditions.

Van Dijke *et al.*²⁸ have suggested a model that connects the macroscopic properties with pore-scale *physics* to determine the saturation-dependency regions of three-phase relative permeabilities. Their work is encouraging, and it may help in finding some general rules (for, say, Eqs. 37 and 38) in practical engineering applications of reservoir simulation.

Miscibility. Previously it was suggested that the gas-water data should be applied together with the gas-oil and oil-water data.¹⁸ In the formulation presented here, the gas-water data is represented by the oil-water data in order to avoid the difficulties with representing the hydrocarbon-water system when gas and oil are miscible. This is especially important for first-contact miscible floods, in which phase labeling changes between gas and oil require continuous functions of capillary pressure and relative permeability.

For the sake of argument, if one assumes that a gas injection process has a compositional path through a critical point (assuming three components, and constant pressure and temperature), it will

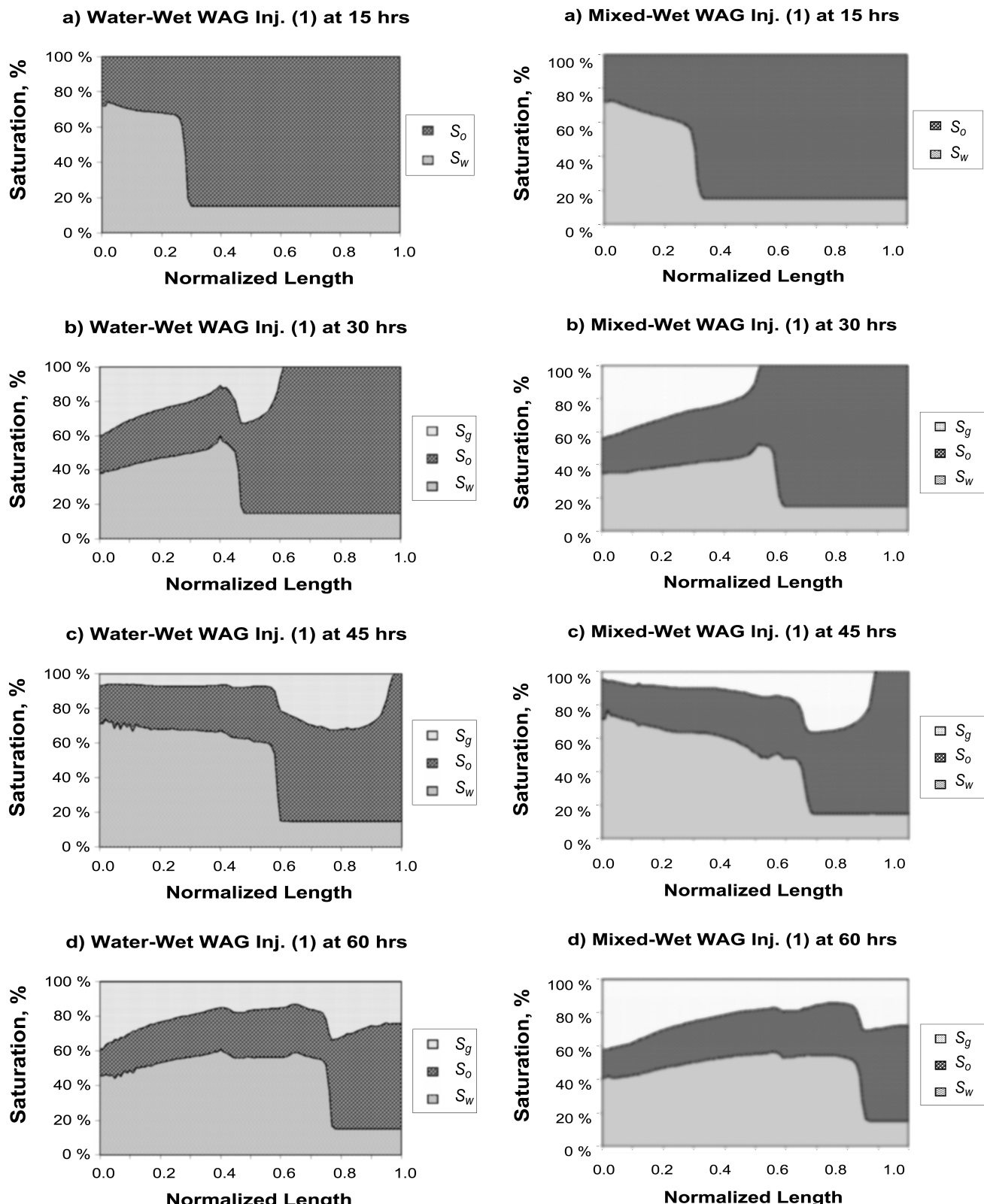


Fig. 6—Saturation profiles for water-wet system.

be a requirement that the input data of Ref. 18 must meet the following criteria (assuming $n_{ij} = 1$):

$$\check{P}_{cgw} = \frac{\check{\sigma}_{gw}^r}{\check{\sigma}_{ow}^r} \check{P}_{cow}, \quad \dots \dots \dots \quad (48)$$

and

$$\check{k}_{rgw} = \frac{\check{\sigma}_{gw}^r}{\check{\sigma}_{ow}^r} (\check{k}_{row} - 1) + 1. \quad \dots \dots \dots \quad (49)$$

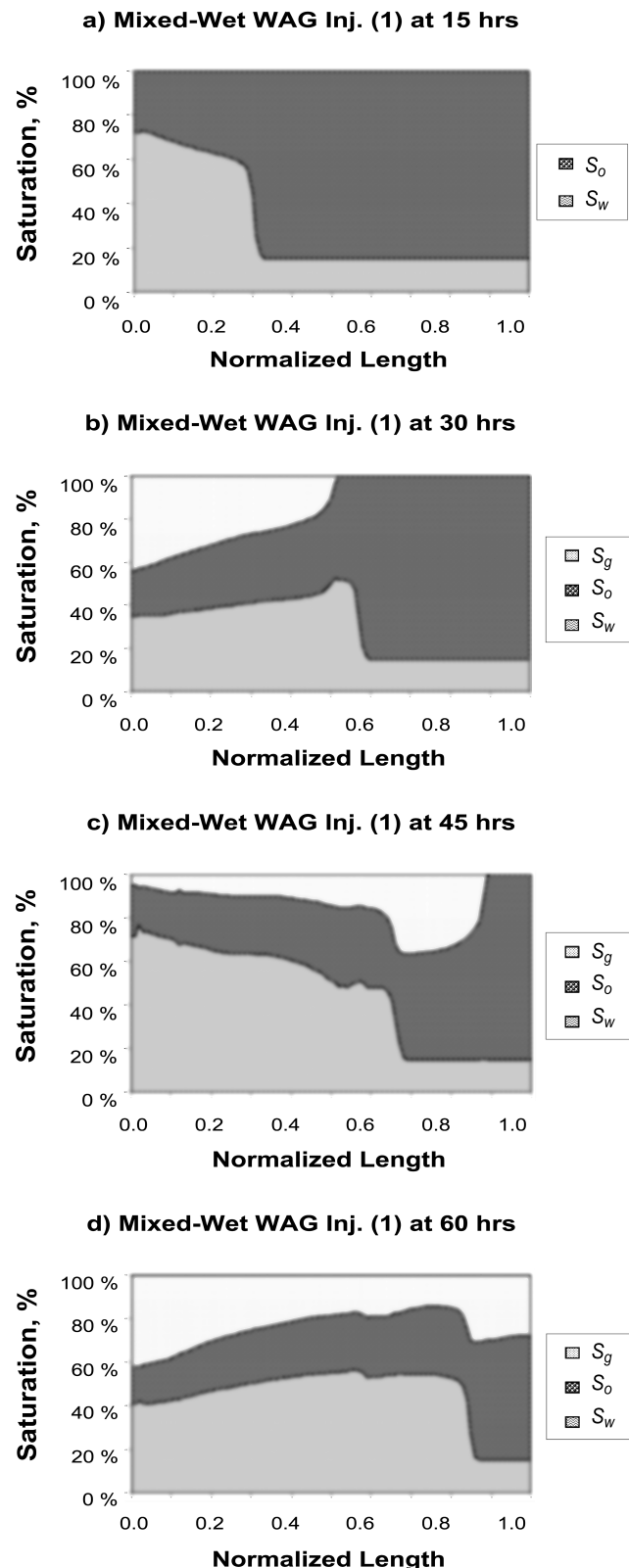


Fig. 7—Saturation profiles for mixed-wet system.

Eqs. 48 and 49 would suffice if the critical state would occur at a unique value of hydrocarbon-water interfacial tension. Because a hydrocarbon system can be miscible at a range of hydrocarbon-water interfacial tension values, these equations are insufficient. Using oil-water properties to represent gas-water properties may also be inappropriate for various fluid systems. It may be necessary to infer an additional function that accounts for the shape changes the oil-water capillary pressure and relative permeability curves will have with varying hydrocarbon-water interfacial tension.

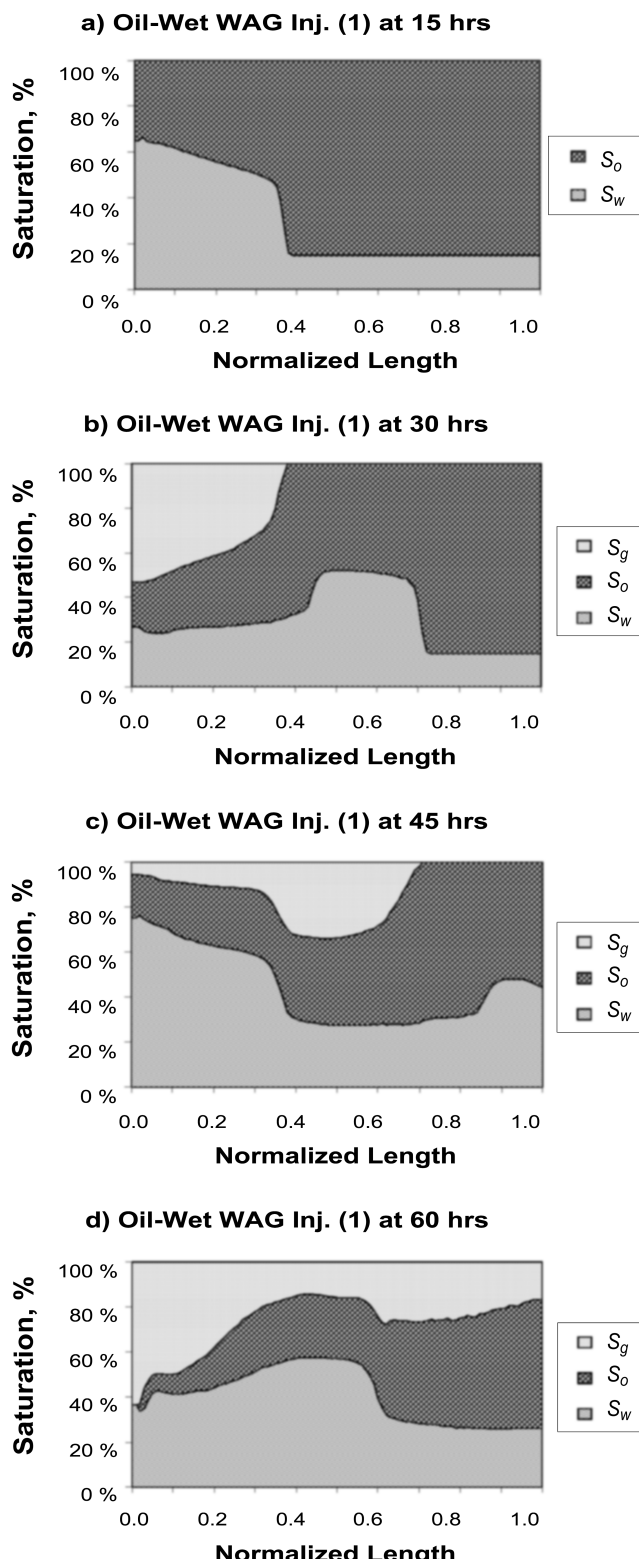


Fig. 8—Saturation profiles for oil-wet system.

Gas-water and oil-water properties must be equivalent at conditions in which the hydrocarbon system is miscible. They must also be equal when the hydrocarbon phase labeling changes at conditions far from a critical state (first-contact miscible). At conditions in which phase labeling changes occur, the phase compositions are discontinuous, and the overall composition is continuous. The interfacial tensions representing the gas-water and oil-water systems will be equal when gas and oil are miscible or have a phase label change. The use of Eq. 9 to scale reference gas-water and oil-water capillary pressure and relative permeability do not

TABLE 3—PARAMETERS IN THE FUNCTIONS F AND H

| Parameters | δ_g | α_g | β_g | δ_g | α_w | β_w |
|------------|------------|------------|-----------|------------|------------|-----------|
| Fig. 9a | 1 | 1 | 1 | 1 | 1 | 1 |
| Fig. 9b | 1 | 3 | 2 | 1 | 0.4 | 4 |

ensure continuity of these functions if the reference interfacial tensions of the two-phase systems are different. To ensure continuous capillary pressure and relative permeability functions when the hydrocarbon phase label change, the oil-water properties have therefore been applied for the gas-water system.

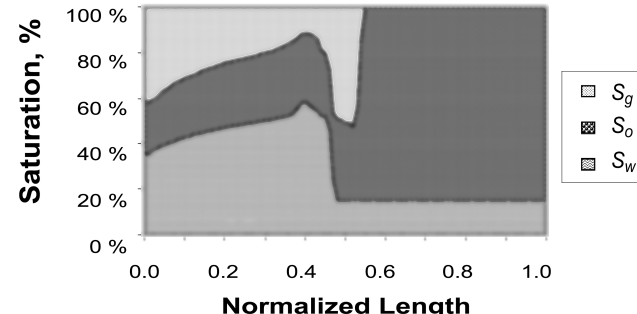
Another issue of importance is the use of table lookup values to model miscible processes. When the hydrocarbon phase label changes, the saturation entries for the gas-water and oil-water functions must coincide in order to ensure continuous hydrocarbon-water capillary pressure and relative permeability.

The question regarding the changing endpoint saturations and functional shapes of capillary pressure and relative permeability as the two-phase fluid system changes from oil-water to gas-water still remains an issue for further investigation. This is also true for, say, the oil-water system undergoing large variations in pressure and temperature.

Fig. 11 illustrates saturation profiles for a first contact miscible WAG injection flood. The same injection procedure is applied here as in the previous examples. The injected gas composition is listed in Table 4. The bottomhole pressure for the producing well and the initial reservoir pressure were raised to 380 bar. The F and H functions were set to zero, and Eqs. 44 and 45 were applied to capillary pressures. These first contact miscible simulations performed without any numerical problems. Simulating the water-wet example with linear functions of F and H (as in Fig. 9a) did not result in any significantly different saturation profiles from those in Fig. 11a.

As a last comment from the examples tested so far, the scaling of these properties with interfacial tensions can have a stronger impact on the saturation profiles compared to the dependence of capillary pressure and relative permeability on saturation.

a) Water-Wet WAG Inj. (2) at 30 hrs



b) Water-Wet WAG Inj. (3) at 30 hrs

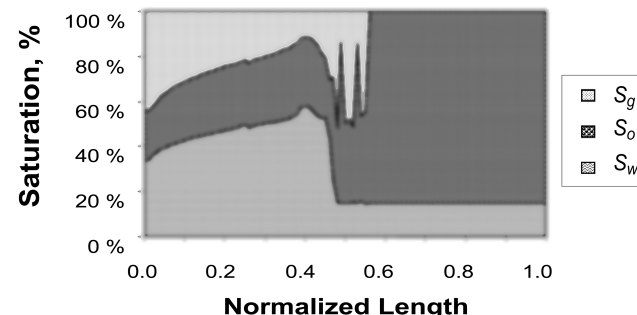


Fig. 9—Saturation profiles using Eqs. 34 and 35.

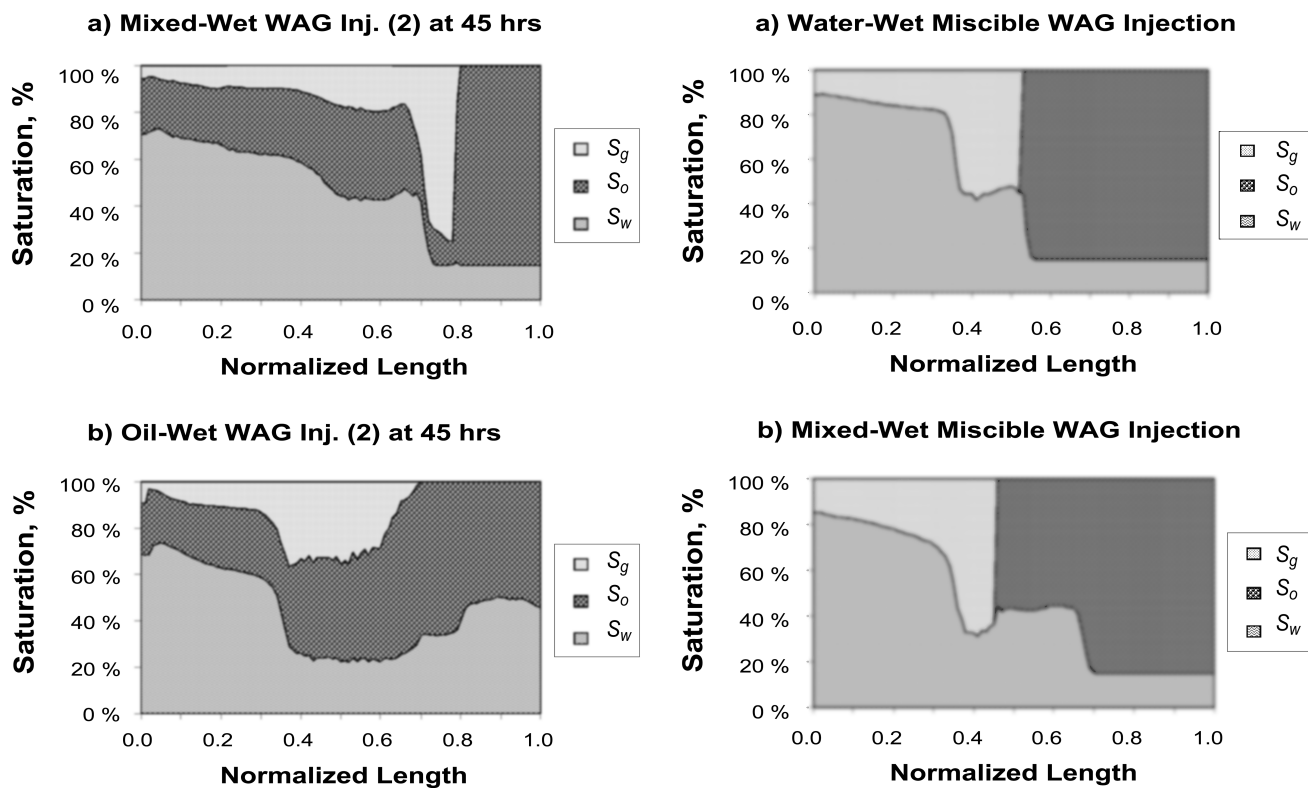


Fig. 10—Saturation profiles for mixed- and oil-wet systems where $P_{cow}(S_o)$ and $P_{cgo}=P_{cgw}(S_w)-P_{cow}(S_o)$.

Conclusions

A consistent and coupled three-phase capillary pressure and relative permeability model has been presented incorporating hysteresis and hydrocarbon miscibility.

The proposed model incorporates varying endpoint saturations for all three phases within the three-phase space. The three-phase capillary-pressure and relative-permeability values are saturation history-dependent.

Test examples have been simulated with the proposed model. The examples consisted of typical capillary pressure and relative permeability data for water-, mixed-, and oil-wet systems. The saturation profiles from the simulations show that the saturation dependency of the capillary pressures has a significant impact on the simulated saturation profiles.

The proposed model, which represents a simple and practical procedure for interpolating two-phase data to obtain three-phase properties, opens for a variety of functional relationships between two-phase and three-phase data. These relationships are subjects for further investigation.

Nomenclature

- A = user-specified constant for hydrocarbon-water IFT
- B = user-specified constant for hydrocarbon-water IFT
- C = user-specified constant for hydrocarbon-water IFT
- f_{ij} = IFT scaling function
- F = correction function for gas-oil capillary pressure
- G = correction function for gas-water capillary pressure
- H = correction function for oil-water capillary pressure
- k_{ri} = input relative permeability to phase i with normalized saturations
- \check{k}_{rij} = input relative permeability to phase i in the presence of phase j
- \check{k}_{rij} = representative relative permeability to phase i
- \hat{k}_{rij} = IFT-scaled representative relative permeability
- n_{ij} = user-specified constant, $i,j=g,o,w$ and $i \neq j$
- p = pressure

a) Water-Wet Miscible WAG Injection

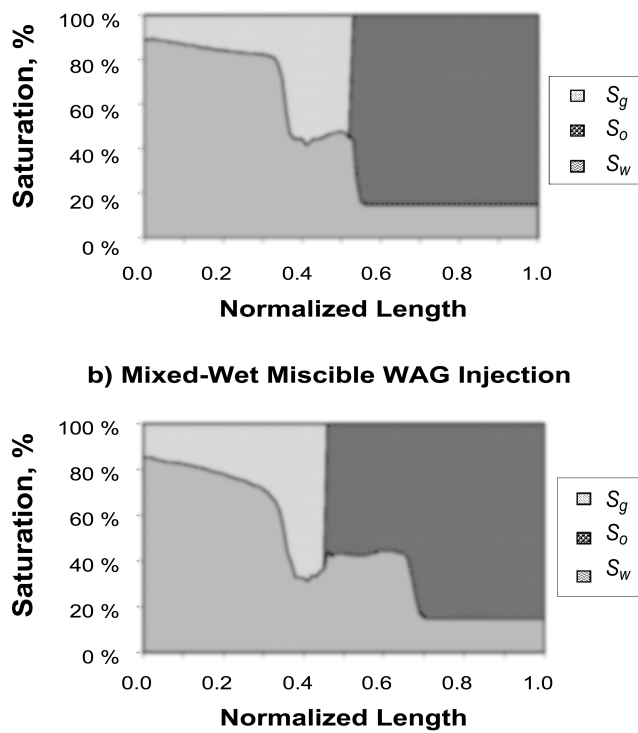


Fig. 11—Saturation profiles for first contact miscible WAG injection at 45 hours for water-, mixed-, and oil-wet systems.

P_{cij} = capillary pressure for phases i and j

\tilde{P}_{cij} = input capillary pressure for phases i and j

\hat{P}_{cij} = representative capillary pressure

\hat{P}_{cij} = IFT-scaled representative capillary pressure

R = capillary pressure constraint residual

S = normalized saturation (input or gridblock)

\check{S} = input saturation

\bar{S} = gridblock saturation

α_i = user-specified constant, $i=g,o,w$

β_i = user-specified constant, $i=g,o,w$

TABLE 4—MISCIBLE INJECTION GAS COMPOSITION

| Component | mol% | Component | mol% |
|-------------------|------|------------------|------|
| N ₂ | 1 | C ₈ | 7 |
| CO ₂ | 3 | HC ₁₃ | 0.4 |
| C ₁ | 63 | HC ₁₈ | 0.3 |
| HC ₂₋₃ | 15 | HC ₂₆ | 0.2 |
| HC ₄₋₇ | 10 | HC ₄₃ | 0.1 |

δ = user-specified constant, = 0 or 1

ρ = mass density

σ_{ij} = interfacial tension between phases i and j

Subscripts

g = gas

gro = gas endpoint in the presence of oil

grw = gas endpoint in the presence of water

imn = minimum for phase i

$imax$ = maximum for phase i

o = oil

org = oil endpoint in the presence of gas

orw = oil endpoint in the presence of water

w = water

wrg = water endpoint in the presence of gas

wro = water endpoint in the presence of oil

Superscripts

d = decreasing

e = equivalent

h = hysteresis

i = increasing

m = scaled

max = maximum

r = reference

t = turning point

Acknowledgments

The Norwegian Research Council and SINTEF Petroleum Research are acknowledged for their financial support.

References

1. *Petroleum Reservoir Simulation*, K. Aziz and A. Settari (eds.), Applied Science Publishers Ltd., London (1979) 29–38.
2. Baker, L.E.: “Three-Phase Relative Permeability Correlations,” paper SPE 17369 presented at the 1988 SPE/DOE Symposium on Enhanced Oil Recovery, Tulsa, 17–20 April.
3. Blunt, M.J.: “An Empirical Model for Three-Phase Relative Permeability,” *SPEJ* (December 2000) 435.
4. Fayers, F.J. *et al.*: “An Improved Three Phase Flow Model Incorporating Compositional Variance,” paper SPE 59313 presented at the 2000 SPE/DOE Improved Oil Recovery Symposium, Tulsa, 3–5 April.
5. Jerauld, G.R.: “General Three-Phase Relative Permeability Model for Prudhoe Bay,” *SPERE* (November 1997) 255.
6. Honarpour, M., Koederitz, L., and Harvey, A.H.: *Relative Permeability of Petroleum Reservoirs*, CRC Press Inc., New York City (1986).
7. Killough, J.E.: “Reservoir Simulation With History-Dependent Saturation Functions,” *SPEJ* (February 1976) 37; *Trans., AIME*, **261**.
8. Larsen, J.A. and Skauge, A.: “Methodology for Numerical Simulation With Cycle-Dependent Relative Permeabilities,” *SPEJ* (June 1998) 163.
9. Anderson, W.G.: “Wettability Literature Survey Part 2: Wettability Measurement,” *JPT* (November 1986) 1246.
10. Anderson, W.G.: “Wettability Literature Survey Part 4: Effects of Wettability on Capillary Pressure,” *JPT* (October 1987) 1283.
11. Anderson, W.G.: “Wettability Literature Survey Part 5: Effects of Wettability on Relative Permeability,” *JPT* (November 1987) 1453.
12. Braun, E.M. and Holland, R.F.: “Relative Permeability Hysteresis: Laboratory Measurements and a Conceptual Model,” *SPERE* (August 1995) 222.
13. Honarpour, M.M., Huang, D.D., and Al-Hussainy, R.: “Simultaneous Measurements of Relative Permeability, Capillary Pressure, and Electrical Resistivity With Microwave System for Saturation Monitoring,” *SPEJ* (September 1996) 283.
14. Kleppe, J. *et al.*: “Representation of Capillary Pressure Hysteresis in Reservoir Simulation,” paper SPE 38899 presented at the 1997 Annual Technical Conference and Exhibition, San Antonio, Texas, 5–8 October.
15. Longeron, D., Kalaydjian, F., and Bardon, C.: “Gas-Oil Capillary Pressure Measurements at Reservoir Conditions: Effects of Interfacial Tension and Connate Water Saturation,” *Proc.*, Seventh European IOR Symposium, Moscow (1993) 466–472.
16. Morrow, N.R. and Harris, C.C.: “Capillary Equilibrium in Porous Materials,” *SPEJ* (March 1965) 15; *Trans., AIME*, **234**.
17. Oak, M.J., Baker, L.E., and Thomas, D.C.: “Three-Phase Relative Permeability of Berea Sandstone,” *JPT* (August 1990) 1054; *Trans., AIME*, **289**.
18. Hustad, O.S. and Hansen, A.-G.: “A Consistent Formulation for Three-Phase Relative Permeabilities and Phase Pressures based on Three Sets of Two-Phase Data,” paper in book *RUTH, A Norwegian Research Program on Improved Oil Recovery, Program Summary*, Norwegian Petroleum Directorate, Stavanger (1996) 183–194; see also *Proc.*, Eighth European Symposium on Improved Oil Recovery, Vienna (1995) 289–298.
19. Mattax, C.C. and Dalton, R.L.: *Reservoir Simulation*. Monograph Series, SPE, Richardson, Texas (1990) **13**, 39.
20. Kjosavik, A., Ringen, J.K., and Skjæveland, S.M.: “Relative Permeability Correlation for Mixed-Wet Reservoirs,” paper SPE 59314 presented at the 2000 SPE/DOE Improved Oil Recovery Symposium, Tulsa, 3–5 April.
21. Stone, H.L.: “Probability Model for Estimating Three-Phase Relative Permeability,” *JPT* (February 1970) 214; *Trans., AIME*, **249**.
22. Hustad, O.S. and Holt, T.: “Gravity Stable Displacement of Oil by Hydrocarbon Gas After Waterflooding,” paper SPE 24116 presented at the 1992 SPE/DOE Symposium on Enhanced Oil Recovery, Tulsa, 22–24 April.
23. Land, C.S.: “Calculation of Imbibition Relative Permeability for Two- and Three-Phase Flow From Rock Properties,” *SPEJ* (June 1968) 149; *Trans., AIME*, **243**.
24. Skaar, B.A.: “Reservoir Simulation of Three-Phase Flow Under Immiscible Flooding With Hysteresis,” Siv.ing. Thesis, The Norwegian U. of Science and Technology, Trondheim (1999).
25. Balibinski, E.F. *et al.*: “Key Characteristics of Three-Phase Oil Relative Permeability Formulations for Improved Oil Recovery Predictions,” *Proc.*, Ninth European Symposium on Improved Oil Recovery, The Hague (1997).
26. Hustad, O.S. and Dalen, V.: “An Explicit Phase-Behavior Model for Pseudocompositional Reservoir Simulation,” *SPE Advanced Technology Series* (1993) **1**, No. 1, 17.
27. Fanchi, J.R.: “Calculation of Parachors for Compositional Simulation: An Update,” *SPERE* (August 1990) 433.
28. Van Dijke, M.I.J., Sorbie, K.S., and McDougall, S.R.: “A Process-Based Approach for Three-Phase Capillary Pressure and Relative Permeability Relationships in Mixed-Wet Systems,” paper SPE 59310 prepared for presentation at the 2000 SPE/DOE Improved Oil Recovery Symposium, Tulsa, 3–5 April.

SI Metric Conversion Factors

| | |
|-----------------------|------------------------|
| bar \times 1.0* | E+05 = Pa |
| cp \times 1.0* | E-03 = Pa·s |
| h \times 3.6 | E+03 = s |
| md \times 9.869 233 | E-04 = μm^2 |

*Conversion factors are exact.

Odd Steve Hustad is a staff engineer at Statoil, e-mail: osh@statoil.com. Previously, he held senior scientist and research director positions at SINTEF Petroleum Research, Reservoir Technology Dept., Trondheim, Norway. He holds a BM degree in applied mathematics from the U. of Waterloo, Ontario, Canada, a Cand. Scient. degree (MS equivalent) in physics from the U. of Trondheim, and a Doktor ingenør degree (PhD equivalent) in petroleum engineering from the Norwegian Inst. of Technology (NTH, now NTNU), Trondheim. He served as 1999/2000 SPE section chairperson in Trondheim.